Electronic Supplementary Material (ESI) for ChemComm.

B_4C nanosheets decorated with in situ-derived boron-doped graphene quantum dots for high-efficiency ambient N_2 fixation

Wei-Bin Qiu,[a] Yu-Xi Luo,[a] Ru-Ping Liang,*[a] Jian-Ding Qiu*[ab] and Xing-Hua Xia*[c]

[a] College of Chemistry, Nanchang University, Nanchang 330031, China.

[b] College of Materials and Chemical Engineering, Pingxiang University, Pingxiang 337055, China.

[c] State Key Laboratory of Analytical Chemistry for Life Science, School of Chemistry and Chemical Engineering, Nanjing University, Nanjing 210023, China.

*Corresponding authors. Tel/Fax: +86-791-83969518. E-mail: rpliang@ncu.edu.cn; jdqiu@ncu.edu.cn; xhxia@nju.edu.cn.

Experimental section

Materials. Sodium nitroferricyanide ($C_5FeN_6Na_2O$) and Nafion 211 membrane were provided by Sigma-Aldrich. Sodium hydroxide (NaOH), salicylic acid ($C_7H_6O_3$), sodium salicylate ($C_7H_5O_3Na$), sodium hypochlorite (NaClO), sodium sulfate (Na_2SO_4), nitric acid (HNO_3), sulfuric acid (H_2SO_4), para-(dimethylamino) benzaldehyde ($C_9H_{11}NO$), hydrochloric acid (HCl), ethanol (C_2H_5OH), and hydrazine (N_2H_4) were purchased from Sinopharm Chemical Reagent Co. Ltd. (China). Boron carbide (B_4C) and Ammonium chloride-^{15}N ($^{15}NH_4Cl$) were purchased from Aladdin Ltd. Dimethyl Sulfoxide-D_6 (DMSO-d_6, 99.9%) was purchased from Adamas Reagent, Ltd. All the chemical regents were of analytical grade and used as received without further purification. Deionized water was purified through a Millipore Milli-Q system.

Preparation of B_4C nanosheet. A 4 g bulk B_4C was dispersed in 100 mL ethanol and stripped by ultrasonic cell disruptor for 1 h. Subsequently, the resulting dispersion was centrifuged for 10 min at 3000 rpm and the supernatant containing B_4C nanosheet was decanted gently. The product was dried in a vacuum at 60 °C.

Preparation of B_4C-BGQDs. B_4C-BGQDs was fabricated by in situ formation of BG on B_4C nanosheets through a structural conversion way followed by cutting of BG into BGQDs. The obtained B_4C nanosheets were subjected to heat treatment (1600 °C) using a single-zone tubular furnace in an inert atmosphere (N_2 gas atmosphere) for 3 h, and were then allowed to cool slowly to room temperature. The BG was cutted into BGQDs by a hydrothermal cutting process.[1] Typically, the as-made powder was first refluxed in 40% HNO_3 for 24 h; after filtration and water washing to neutral, the product was dried in a vacuum at 60 °C. Then, the product was heated to 300 °C with a heating rate of 5 °C/min and then maintained at 300 °C for 2 h in a tube furnace under an argon atmosphere. The sample was oxidized with concentrated H_2SO_4 and HNO_3 (volume ratio 1:3) for 17 h under mild ultrasonication without any pausing. The solution was separated and collected by centrifugation (5000 rpm for 20 min), followed by washing with ethanol, and then redispersed in 40 mL of ultrapure water. The pH was adjusted to 8 with NaOH. The solution was then put into a poly(tetrafluoroethylene) (Teflon)-lined autoclave and heated at 200 °C for 11.5 h.

The precipitate was collected and washed with water and ethanol for several times by centrifugation and dried at 60 °C. The supernatant containing BGQDs was further characterized by fluorescence spectrum and atomic force microscopy (AFM) to confirm the formation of BGQDs.

Characterization. Fluorescence spectrum was obtained using an F-7000 fluorescence spectrometer (Hitachi, Japan). AFM image was collected on a Bruker Multimode 8 AFM/SPM (Bruker, Germany) system with NanoScope Analysis Version 1.40 software. The X-ray diffraction analysis (XRD) was performed on a Bruker D8 Advance X-ray diffractometer with Cu Kα (α = 1.5405 Å) radiation. JEOL2010 transmission electron microscope (TEM, Japan) was used to characterize the size and morphology of B_4C-BGQDs. Raman spectrum was collected using a Renishaw InVia micro-Raman (Renishaw, UK) system with the excitation wavelength at 514 nm. The absorbance data of spectrophotometer were measured on an UV-2450 spectrophotometer (Shimadzu, Japan). X-ray photoelectron spectroscopy (XPS) characterizations were measured by a VG Multilab 2000X instrument (Thermal Electron, USA). N_2 temperature programmed desorption (N_2-TPD) was measured with a Micromeritics AutoChem 2920 apparatus to ascertain the N_2 adsorption ability of the catalysts. Briefly, 40 mg of the catalyst was first pre-treated with pure He at a flow rate of 50 mL·min^{-1} at 120 °C for 30 min, followed by cooling down to room temperature under the same atmosphere and then dosed with pure N_2. To remove residual N_2, the catalyst was purged with pure He at a flow rate of 50 mL·min^{-1} for 30 min. The N_2-TPD measurement was subsequently performed up to 600 °C at a heating rate of 10 °C·min^{-1} in pure He. A gas chromatograph (SHIMADZU, GC-2014C) equipped with MolSieve 5A column and Ar carrier gas was used for the periodic quantification of H_2 during NRR tests using B_4C-BGQDs/CPE

Electrochemical measurement. The reduction of N_2 gas (99.99%) was carried out in a two-compartment cell under ambient condition, which was separated by a Nafion 211 membrane. Before NRR tests, the membrane was protonated by first boiling in ultrapure water for 1 h and treating in H_2O_2 (5%) aqueous solution at 80 °C for another 1 h. Finally, the membrane was treated in 0.5 M H_2SO_4 at 80 °C for 3 h and in

water for 6 h. Electrochemical measurements were performed with an Iviumstat electrochemical workstation (Eco Chemie, Netherlands) in a standard three-electrode system using B_4C-BGQDs as the working electrode, Ag/AgCl as the reference, and a graphite rod as the counter electrode. All experiments were carried out at room temperature (25 °C). To acquire the ESA of the working electrodes, their roughness factor (Rf) should be obtained firstly according to the equation: $ESA=R_fS$, where S was generally equal to the geometric area of carbon paper electrode (In this work, S=1 cm^{-2}). The R_f was determined by the relation $Rf=C_{dl}/30$ μF cm^{-2} based on the double-layer capacitance (C_{dl}) of a smooth metal-free surface (30 μF cm^{-2}).[2] The C_{dl} was determined by measuring the capacitive current associated with double-layer charging from the scan-rate dependence of cyclic voltammetric stripping. For this, the potential window of cyclic voltammetric stripping was −0.25 V to −0.15 V (0.1 M HCl solution). The scan rates were 10 mV s^{-1}, 20 mV s^{-1}, 50 mV s^{-1}, 100 mV s^{-1}. The C_{dl} was estimated by plotting the $\Delta j=(j_a-j_c)$ at −0.2 V (where j_c and j_a are the cathodic and anodic current densities, respectively) against the scan rate, in which the slope was twice that of C_{dl}.[3] Electrochemical impedance spectroscopy (EIS) tests were performed in a 0.1 M HCl solution at –0.45 V in the frequency range from 0.1 to 10^6 Hz. Linear sweep voltammogram (LSV) tests were performed in a 0.1 M HCl solution at a scan rate of 5 mV s^{-1}. The provided LSV curves were the steady-state ones after several cycles. For N_2 reduction experiments, the cathode chamber was first purged with N_2 for 30 min before measurement to form N_2-saturated solution, then conducted in 0.1 M HCl with continuous N_2 bubbling. All potentials (E) in this study were recorded on a reversible hydrogen electrode (RHE) by the equation:

$$E_{RHE} = E_{Ag/AgCl} + 0.059\ pH + 0.256\ V \qquad (S\text{-}1)$$

Determination of NH_3. The concentration of produced NH_3 was determined by the indophenol blue method.[4] In detail, 2 mL HCl electrolyte was taken from the cathodic chamber, and then 2 mL of 1 M NaOH solution containing 5% $C_7H_6O_3$ and 5% $C_7H_5O_3Na$ were added into this solution. Subsequently, 1 mL of 0.05 M NaClO and 0.2 mL of 1% $C_5FeN_6Na_2O{\cdot}2H_2O$ were added into the above solution. After standing

at room temperature for 2 h, UV-Vis absorption spectrum was measured at a wavelength of 655 nm. The concentration-absorbance curves were calibrated using the standard NH_3 solution with a series of concentrations. The fitting curve (Fig. S5, y = 0.330x + 0.009, R^2 = 0.999) shows good linear relation of the absorbance value with NH_3 concentration by three times independent calibrations.

Determination of N_2H_4. The N_2H_4 concentration in the electrolyte was estimated by the method of Watt and Chrisp.[5] In brief, a mixture solution containing $C_9H_{11}NO$ (5.99 g), concentrated HCl (30 mL) and C_2H_5OH (300 mL) was used as a color reagent. Then, 5 mL of electrolyte after electrolysis was added into the 5 mL of above color reagent with stirring at room temperature for 20 min. The absorbance of the resulting solution was measured by an UV-Vis spectrophotometer at a wavelength of 455 nm. The concentration-absorbance curve was calibrated using standard N_2H_4 solutions with a series of concentrations (0−0.6 μg ml^{-1}) for three independent calibrations. The fitting curve (Fig. S6 , y = 0.900x + 0.026, R^2 = 0.999) shows good linear relation of absorbance value with N_2H_4 concentration by three times independent calibrations.

$^{15}N_2$ Isotope Labeling Experiments. The isotopic labeling experiment was carried out using $^{15}N_2$ as the feeding gas (Sigma-Aldrich, 98 atom % $^{15}N_2$) with 0.1 M HCl electrolyte. After $^{15}N_2$ electroreduction for 2 h at −0.45 V (vs. RHE), the electrolyte was taken out and concentrated to 1 mL by a rotary evaporator at 70 °C. Afterwards, 0.9 mL of the resulting solution was taken out and mixed with 0.1 mL DMSO-d_6 as an internal standard for ^{1}H nuclear magnetic resonance measurement (^{1}H NMR, Bruker Avance III 600 MHz).

Calculations of NH_3 yield and Faradaic efficiency (FE). The FE for N_2 reduction was defined as the amount of electric charge used for synthesizing NH_3 divided by the total charge passed through the electrodes during the electrolysis. The total amount of NH_3 produced was measured using a colorimetric method. Assuming three electrons were needed to produce one NH_3 molecule, the rate of NH_3 formation (v_{NH_3}) was calculated using the following equation:

$$v_{NH_3} = \frac{C_{NH_3} \times V}{t \times m_{cat.}} \quad \text{(S-2)}$$

The FE for NH_3 formation (FE_{NRR}) could be calculated as follows:

$$FE_{NRR} = \frac{3 \times F \times C_{NH_3} \times V}{17 \times Q} \quad \text{(S-3)}$$

where, F is the Faraday constant, C_{NH_3} is the measured NH_3 concentration, V is the volume of the HCl electrolyte for NH_3 collection, t is the reduction time (2 h) and $m_{cat.}$ is the catalyst loading mass, Q is the total charge passed through the electrode (C).

FE for H_2 (FE_{HER}) was calculated according to following equation:

$$FE_{HER} = 2 \times F \times n/Q \quad \text{(S-4)}$$

where F is the Faraday constant, n is the actually produced H_2 (mol), and Q is the total charge passed through the electrode (C).

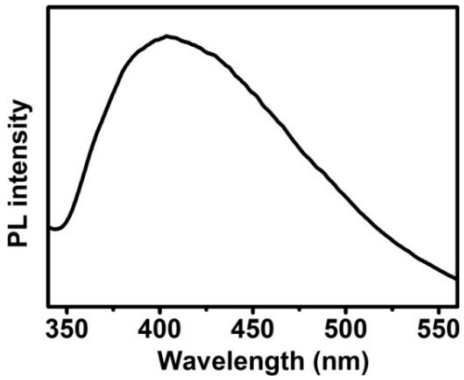

Fig. S1. Photoluminescence spectrum of BGQDs with a 310 nm excitation beam.

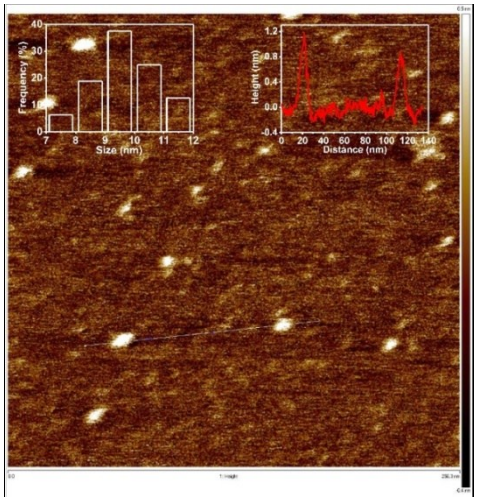

Fig. S2. AFM image of the dispersive BGQDs deposited on a freshly cleaved mica. The insets show a particle size histogram (left inset) and the height distribution of the BGQDs (right inset). The average particle size of BGQDs is about 10 nm.

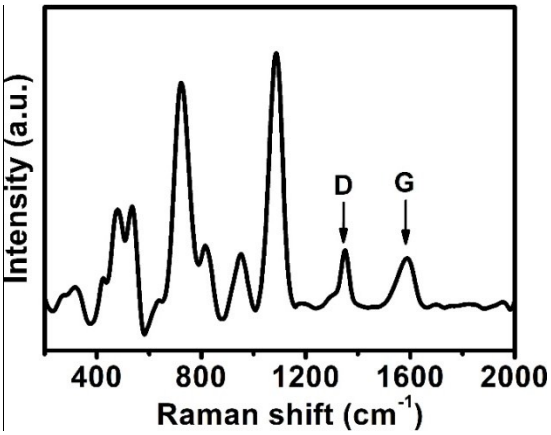

Fig. S3. Raman spectrum of B_4C-BGQDs.

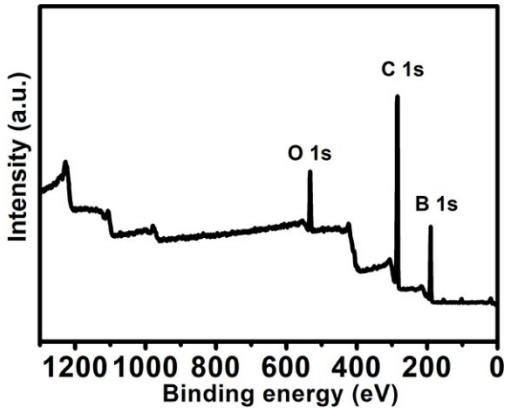

Fig. S4. XPS survey spectra of B_4C-BGQDs.

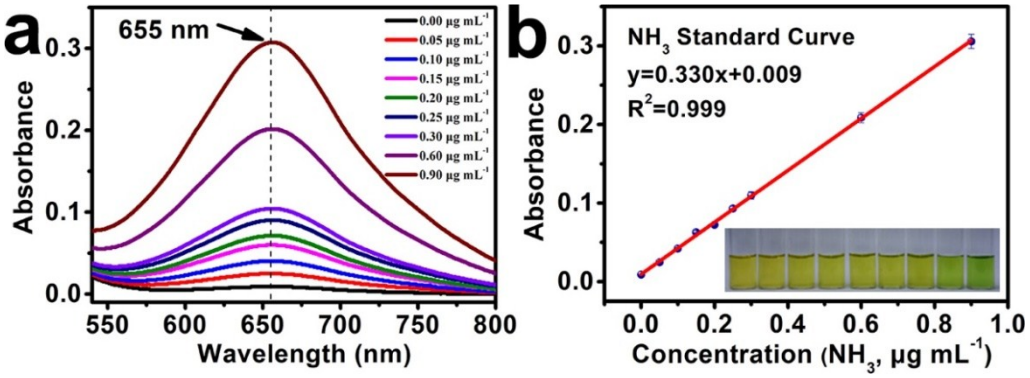

Fig. S5. Absolute calibration of the indophenol blue method using ammonium chloride solutions with a series of NH_3 concentrations as standard. (a) UV-Vis absorption spectra of indophenol assays with NH_3 after incubated at room temperature

for 2 h. (b) Calibration curve (y = 0.330x + 0.009, R^2 = 0.999) used for estimation of NH_3. The inset in (b) shows the chromogenic reaction of indophenol indicator with NH_3.

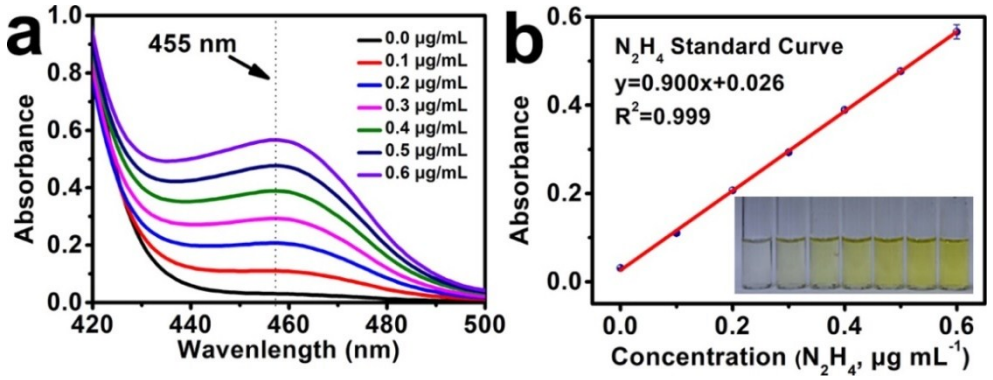

Fig. S6. Absolute calibration of the Watt and Chrisp method for estimating N_2H_4 concentration, using N_2H_4 solutions with known concentration as standard. (a) UV-Vis absorption spectra of various N_2H_4 concentration after incubated at room temperature for 20 min. (b) Calibration curve (y = 0.900x + 0.026, R^2 = 0.999) used for calculation of N_2H_4 concentration. The inset in (b) shows the chromogenic reaction of para-dimethylamino-benzaldehyde indicator with $N_2H_4 \cdot H_2O$.

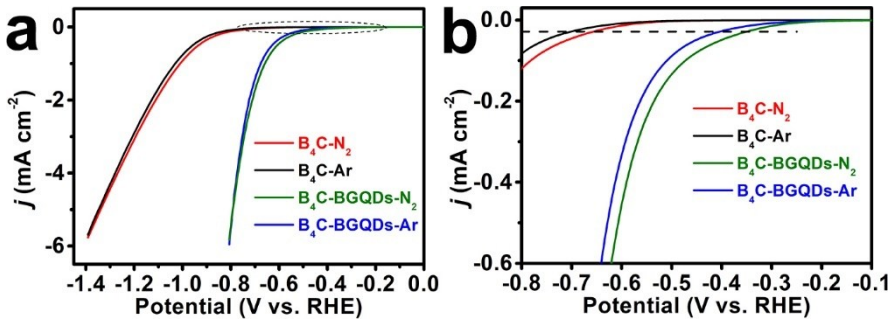

Fig. S7. (a) Linear sweep voltammograms (sweep rate 5 mV s^{-1}) of B_4C nanosheets/CPE and B_4C-BGQDs/CPE electrode recorded in N_2-saturated and Ar-saturated 0.1 M HCl solution respectively. (b) A magnified view of the dotted line part in (a).

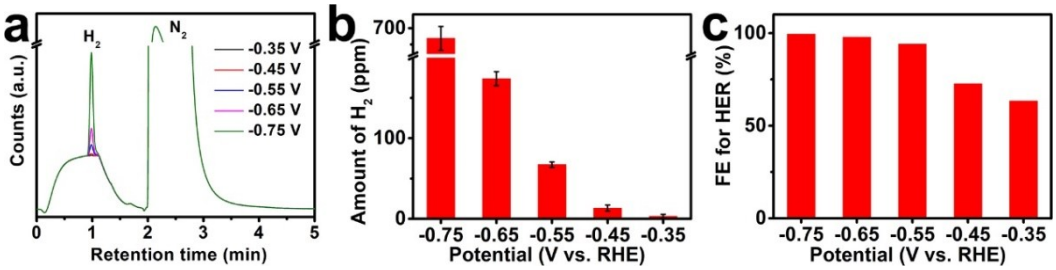

Fig. S8. (a) Gas chromatography (GC) spectra of as-generated gas for the NRR on B_4C-BGQDs/CPE catalyst in N_2-saturated 0.1 M HCl at various potentials, (b) Amounts of H_2 and (c) the calculated FEs of hydrogen evolution reaction (HER) accordingly.

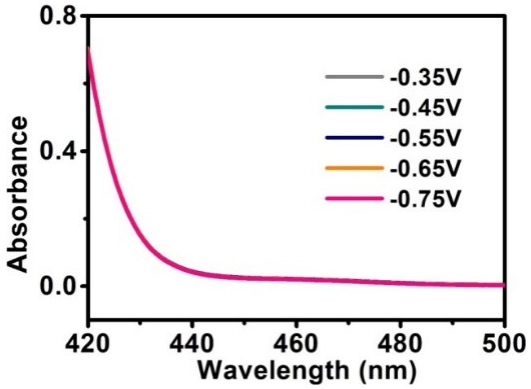

Fig. S9. UV-Vis absorption spectra of the electrolytes stained with para-(dimethylamino) benzaldehyde indicator after electrolysis at a series of potentials for 20 min.

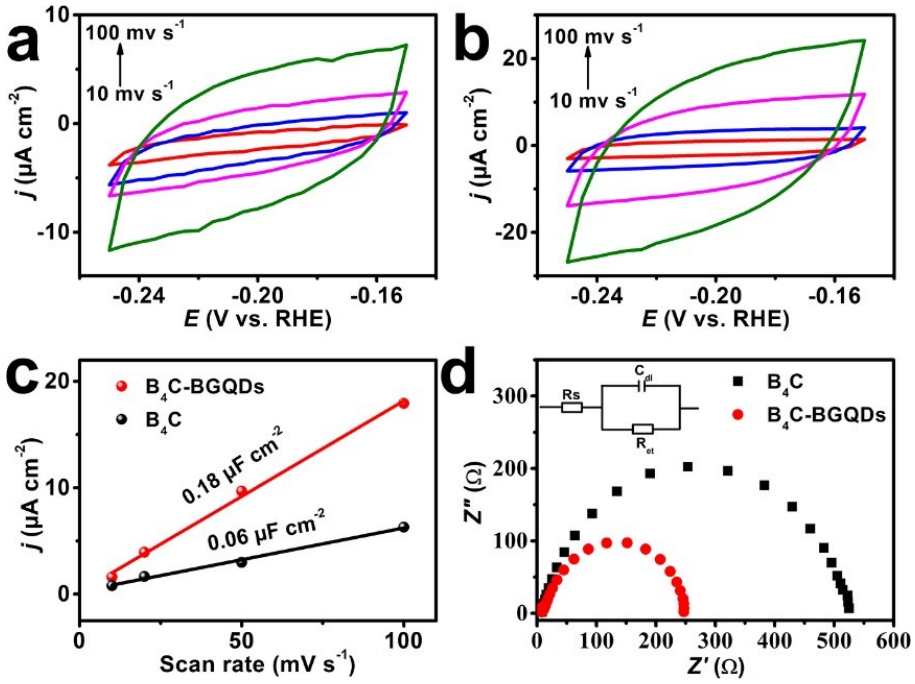

Fig. S10. CV curves for (a) B_4C nanosheets/CPE and (b) B_4C-BGQDs/CPE at scan rates of 10, 20, 50, and 100 mV s^{-1}. (c) Corresponding capacitive currents at –0.2 V as a function of scan rate for B_4C nanosheets/CPE and B_4C-BGQDs/CPE. (d) Nyquist plots of B_4C nanosheets/CPE and B_4C-BGQDs/CPE at –0.45 V in the frequency

range from 0.1 to 10^6 Hz. Inset shows the equivalent circuit used to model the impedance data. All experiments were carried out in 0.1 M HCl.

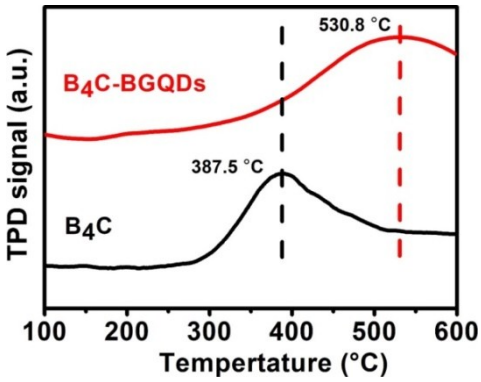

Fig. S11. N_2-TPD profiles of B_4C and B_4C-BGQDs.

To verify the effective NH_3 molecules detected mainly from the electrocatalyzed conversion of N_2 over B_4C-BGQDs/CPE, some necessary control experiments were carried out. Specifically, we performed electrolysis in N_2-saturated 0.1 M HCl solution at an open circuit potential and in Ar-saturated electrolyte at −0.45 V (Fig. S12). Specifically, no apparent NH_3 is detected in the electrolyte after two hours of electrolysis when N_2 is replaced by Ar and at open circuit potential, indirectly indicating that the detected NH_3 stems only from NRR catalyzed by B_4C-BGQDs/CPE. Moreover, the time-dependent experiment shows that the production of NH_3 actually increases with the reaction time, further confirming that NH_3 molecules mainly originate from N_2 (Fig. S13). Furthermore, ^{15}N isotopic labeling experiment was performed as an alternative method to verify the N source of the produced NH_3 in 0.1 M HCl electrolyte. A triplet coupling for $^{14}NH_4^+$ and a doublet coupling for $^{15}NH_4^+$ in the ^1H nuclear magnetic resonance (1H NMR) spectra are used to distinguish them. As shown in Fig. S14, only $^{15}NH_4^+$ was observed in the electrolyte when $^{15}N_2$ was supplied as the feeding gas, and no NH_4^+ was detected when Ar was supplied, which are consistent with the control experiments and confirm that the NH_3 was produced by B_4C-BGQDs/CPE-catalyzed electroreduction of N_2.

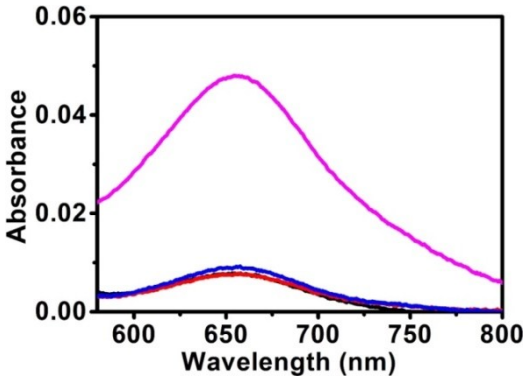

Fig. S12. UV-Vis absorption spectra of the electrolytes stained with indophenol indicator for B_4C-BGQDs/CPE under different conditions. (Color code: black curve, pure electrolyte solution; red curve: N_2-saturated solution at open circuit potential for 2 h; blue dotted curve: electrolysis in Ar-saturated solution at −0.45 V for 2 h; pink curve: electrolysis in N_2-saturated solution at −0.45 V for 2 h.)

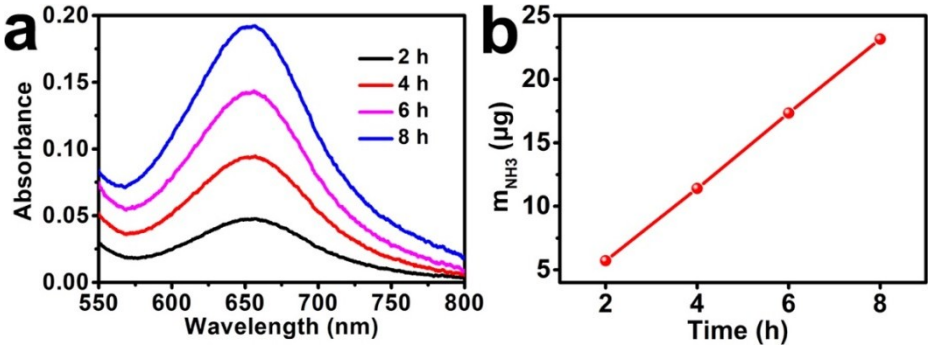

Fig. S13. (a) UV-vis absorption spectra of HCl electrolyte after electrolysis on B_4C-BGQDs/CPE stained with indophenol indicator after charging for different interval times at –0.45 V. (b) The corresponding curve of NH_3 amount *vs*. reaction time in 0.1 M HCl at –0.45 V.

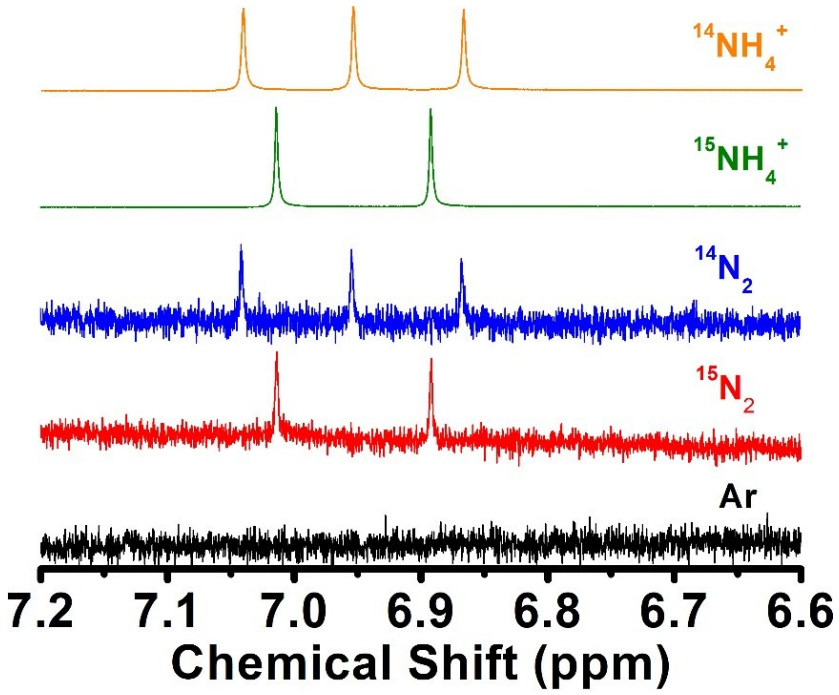

Fig. S14. ^{1}H NMR spectra were obtained for the post-electrolysis 0.1 M HCl electrolytes with $^{15}N_2$, $^{14}N_2$, or Ar as the feeding gas. In the ^{1}H NMR spectra, a doublet coupling for $^{15}NH_4^+$ and a triplet coupling for $^{14}NH_4^+$ were distinguished for the $^{15}N_2$- and $^{14}N_2$-saturated electrolytes after electrolysis, confirming that the NH_3 was produced from the feeding gas. No apparent signals were observed when the electrolyte was bubbled with Ar, indicating a negligible amount of background NH_3 from the catalyst, the electrolyte or the environment, which is consistent with the control experiment using the indophenol blue method in Fig. S8.

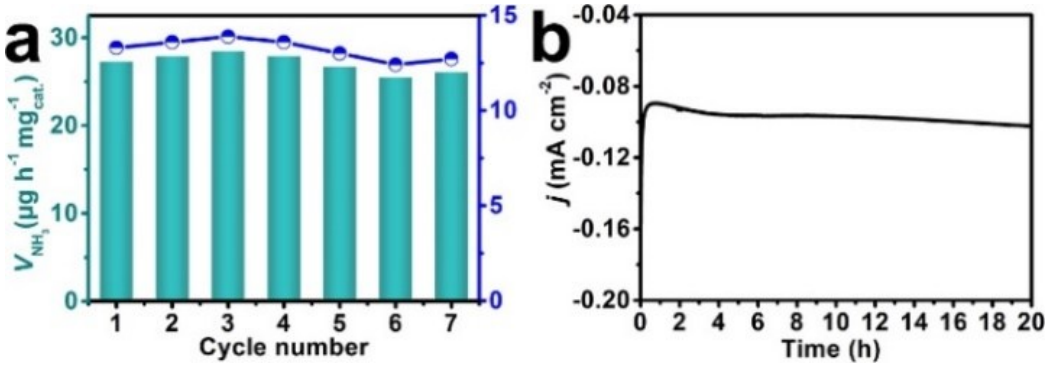

Fig. S15. (a) Cycling test of B_4C-BGQDs/CPE at −0.45 V. (b) Chronoamperometry curve of B_4C-BGQDs/CPE for NRR at −0.45 V for 20 h.

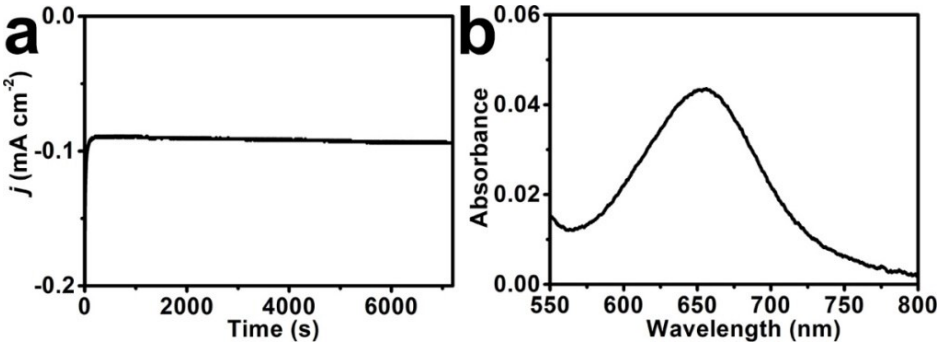

Fig. S16. (a) Chronoamperometry curve of B_4C-BGQDs/CPE after 20-h electrolysis at −0.45 V. (b) UV-Vis absorption spectrum of the corresponding electrolyte.

Table S1. Comparison of the electrocatalytic N_2 reduction performance for B_4C nanosheet with other recently reported the-state-of-art electrocatalysts under ambient conditions.

Catalyst	Electrolyte	V_{NH3}	FE (%)	Potential (V vs. RHE)	Ref.
Metal-free NRR electrocatalysts					
B_4C-BGQDs/CPE	**0.1 M HCl**	**28.6 μg h^{-1} mg^{-1}** **2.86 μg h^{-1} cm^{-2}**	**16.7**	**V_{NH3}: −0.45** **FE: −0.35**	**This work**
B_4C/CPE	0.1 M HCl	26.57 μg h^{-1} mg^{-1}	15.95	−0.75	6
Boron-doped graphene	0.05 M H_2SO_4	9.8 μg h^{-1} cm^{-2}	10.8	−0.5	7
PCN-NVs	0.1 M HCl	8.09 μg h^{-1} mg^{-1}	11.59	−0.2	8
Black phosphorus nanosheets	0.01 M HCl	31.37 μg h^{-1} mg^{-1}	5.07	V_{NH3}: −0.7 FE: −0.6	9
NCM	0.1 M HCl	8 μg h^{-1} cm^{-2}	5.2	V_{NH3}: −0.3 FE: −0.2	10
CC-450	0.1 M Na_2SO_4 +0.02 M H_2SO_4	15.85 μg h^{-1} cm^{-2}	6.92	−0.3	11
NPC-500	0.005 M H_2SO_4	22.3 μg h^{-1} cm^{-2}	9.98	−0.4	12
PEBCD/C	0.5 M Li_2SO_4	1.58 μg h^{-1} cm^{-2}	2.85	−0.5	13
N-doped porous carbon	0.05 M H_2SO_4	23.80 μg h^{-1} mg^{-1}	1.42	−0.9	14
ZIF-derived carbon	0.1 M KOH	57.8 μg h^{-1} cm^{-2}	10.20	−0.3	15
N-doped carbon nanospikes	0.25 M $LiClO_4$	97.18 μg h^{-1} cm^{-2}	11.56	−1.19	16
Boron Nanosheet	0.1 M Na_2SO_4	13.22 μg h^{-1} mg^{-1}	4.04	-0.8	17
S dots-graphene nanohybrid	0.5 M LiClO4	28.56 μg h^{-1} mg^{-1}	7.07	-0.85	18
BCN	0.1 M HCl	7.75 μg h^{-1} mg^{-1}	13.79	-0.3	19
Metal-based NRR electrocatalysts					
TA-reduced Au/TiO_2	0.1 M HCl	21.4 μg h^{-1} mg^{-1}	8.11	−0.2	20
α-Au/CeO_x-RGO	0.1 M HCl	8.31 μg h^{-1} mg^{-1}	10.1	−0.2	21

AuHNCs	0.5 M $LiClO_4$	3.90 μg h^{-1} cm^{-2}	30.2	V_{NH3}: −0.5 FE: −0.4	22
Ag-Au@ZIF	THF-based electrolyte	0.61 μg h^{-1} cm^{-2}	18	N/A	23
Pd/C	0.1 M PBS	4.5 μg h^{-1} mg^{-1}	8.2	0.1	24
Ru/C	2 M KOH	0.21 μg h^{-1} cm^{-2}	0.28	−1.1	25
Ru SAs/N-C	0.05 M H_2SO_4	120.9 μg h^{-1} mg^{-1}	29.6	-0.2	26
BiNCs/CB/CP	K_2SO_4 (pH=3.5)	3400 μg h^{-1} mg^{-1}	66	-0.6	27
CoO QD/RGO	0.1 M Na_2SO_4	21.5 μg h^{-1} mg^{-1}	8.3	-0.6	28
Fe_{SA}–N–C	0.1M KOH	7.48 μg h^{-1} mg^{-1}	56.55	0	29

References

1 L. Zhang, Z.-Y. Zhang, R.-P. Liang, Y.-H. Li and J.-D. Qiu, *Anal. Chem.*, 2014, **86**, 4423–4430.

2 A. Chakraborty, R. Devivaraprasad, B. Bera and M. Neergat, *Phys. Chem. Chem. Phys.*, 2017, **19**, 25414–25422.

3 S. Gao, X. Jiao, Z. Sun, W. Zhang, Y. Sun, C. Wang, Q. Hu, X. Zu, F. Yang and S. Yang, *Angew. Chem., Int. Ed.*, 2016, **55**, 698–702.

4 D. Zhu, L. Zhang, R. E. Ruther and R. J. Hamers, *Nat. Mater.*, 2013, **12**, 836−841.

5 G. W. Watt and J. D. Chrisp, *Anal. Chem.*, 1952, **24**, 2006−2008.

6 W. Qiu, X. Xie, J. Qiu, W. Fang, R. Liang, X. Ren, X. Ji, G. Cui, A. M. Asiri, G. Cui, B. Tang and X. Sun, *Nat. Commun.,* 2018, **9**, 3485.

7 X. M. Yu, P. Han, Z. X. Wei, L. S. Huang, Z. X. Gu, S. J. Peng, J. M. Ma and G. F. Zheng, *Joule,* 2018, ***2***, 1610–1622.

8 C. D. Lv, Y. M. Qian, C. S. Yan, Y. Ding, Y. Y. Liu, G. Chen and G. H. Yu, *Angew. Chem., Int. Ed.*, 2018, ***57***, 10246–10250.

9 L. Zhang, L.-X. Ding, G.-F. Chen, X. Yang and H. Wang, *Angew. Chem., Int. Ed.*, 2019, **58**, 2612–2616.

10 H. Wang, L. Wang, Q. Wang, S. Ye, W. Sun, Y. Shao, Z. Jiang, Q. Qiao, Y. Zhu, P. Song, D. Li, L. He, X. Zhang, J. Yuan, T. Wu and G. A. Ozin, *Angew. Chem., Int. Ed.,* 2018, **57**, 12360–12364.

11 W. Li, T. Wu, S. Zhang, Y. Liu, C. Zhao, G. Liu, G. Wang, H. Zhang and H. Zhao, *Chem. Commun.,* 2018, **54**, 11188−11191.

12 C. Zhao, S. Zhang, M. Han, X. Zhang, Y. Liu, W. Li, C. Chen, G. Wang, H. Zhang and H. Zhao, *ACS Energy Lett.,* 2019, **4**, 377−383.

13 G.-F. Chen, X. Cao, S. Wu, X. Zeng, L.-X. Ding, M. Zhu and H. Wang, *J. Am. Chem. Soc.,* 2017, **139**, 9771–9774.

14 Y. Liu, Y. Su, X. Quan, X. Fan, S. Chen, H. Yu, H. Zhao, Y. Zhang and J. Zhao, *ACS Catal.*, 2018, **8**, 1186−1191.

15 S. Mukherjee, D. A. Cullen, S. Karakalos. K. X. Liu, H. Zhang, S. Zhao, H. Xu, K. L. More, G. F. Wang and G. Wu, *Nano Energy,* 2018, **48**, 217–226.

16 Y. Song, D. Johnson, R. Peng, D. K. Hensley, P. V. Bonnesen, L. Liang, J. Huang, F. Yang, F. Zhang, R. Qiao, A. P. Baddorf, T. J. Tschaplinski, N. L. Engle, M. C. Hatzell, Z. Wu, D. A. Cullen, H. M. Meyer, B. G. Sumpter and A. J. Rondinone, *Sci. Adv.,* 2018, **4**, e1700336.

17 X. Zhang, T. Wu, H. Wang, R. Zhao, H. Chen, T. Wang, P. Wei, Y. Luo, Y. Zhang and X. Sun, *ACS Catal.*, 2019, **9**, 4609–4615.
18 H. Y. Chen, X. J. Zhu, H. Huang, H. B. Wang, T. Wang, R. B. Zhao, H. G. Zheng, A. M. Asiri, Y. L. Luo and X. P. Sun, *Chem. Commun.*, 2019, **55**, 3152–3155.
19 C. Chen, D. Yan, Y. Wang, Y. Zhou, Y. Zou, Y. Li and S. Wang, *Small*, 2019, **15**, 1805029.
20 M. Shi, D. Bao, B. Wulan, Y. Li, Y. Zhang, J. Yan and Q. Jiang, *Adv. Mater.,* 2017, **29**, 1606550.
21 S. Li, D. Bao, M. Shi, B. Wulan, J. Yan and Q. Jiang, *Adv. Mater.,* 2017, **29**, 1700001.
22 M. Nazemi, S. R. Panikkanvalappil and M. A. El-Sayed, *Nano Energy,* 2018, **49**, 316–323.
23 H. K. Lee, C. S. L. Koh, Y. H. Lee, C. Liu, I. Y. Phang, X. Han, C.-K. Tsung and X. Y. Ling, *Sci. Adv.*, 2018, **4**, eaar3208.
24 J. Wang, L. Yu, L. Hu, G. Chen, H. Xin and X. Feng, *Nat. Commun*., 2018, **9**, 1795.
25 V. Kordali, G. Kyriacou and C. Lambrou, *Chem. Commun.*, 2000, **0**, 1673–1674.
26 Z. Geng, Y. Liu, X. Kong, P. Li, K. Li, Z. Liu, J. Du, M. Shu, R. Si and J. Zeng, *Adv. Mater.*, 2018, **30**, 1803498.
27 Y.-C. Hao, Y. Guo, L.-W. Chen, M. Shu, X.-Y. Wang, T.-A. Bu, W.-Y. Gao, N. Zhang, X. Su, X. Feng, J.-W. Zhou, B. Wang, C.-W. Hu, A.-X. Yin, R. Si, Y.-W. Zhang and C.-H. Yan, *Nat. Catal.*, 2019, **2**, 448–456.
28 K. Chu, Y.-p. Liu, Y.-b. Li, H. Zhang and Y. Tian, *J. Mater. Chem. A*, 2019, **7**, 4389–4394.
29 M. Wang, S. Liu, T. Qian, J. Liu, J. Zhou, H. Ji, J. Xiong, J. Zhong and C. Yan, *Nat. Commun*., 2019, **10**, 341.